Separating atmospheric and ocean-mediated impacts of time-evolving industrial and biomass burning aerosols on historical boreal summer climate

Xueying Zhao[a,b*], Clara Deser[a], Geeta Persad[b], Adam S. Phillips[a], Kayla White[b], and Nan Rosenbloom[a]

[a] *NSF National Center for Atmospheric Research, Boulder CO*

[b] *Jackson School of Geosciences, The University of Texas at Austin, Austin TX*

* *Corresponding author*: Dr. Xueying Zhao, Climate and Global Dynamics Laboratory, NCAR, 1850 Table Mesa Drive, Boulder CO 80305, xueying.zhao@jsg.utexas.edu

Submitted to *Journal of Climate*

File generated with AMS Word template 2.0

ABSTRACT

The spatial pattern of industrial aerosol emissions has changed markedly over the past century, alongside regional shifts in biomass burning (BMB) sources. While previous studies examined evolving industrial aerosol effects, the relative contributions of atmospheric radiative *vs.* ocean-mediated responses to combined aerosol sources remain unclear. Using global atmosphere-land simulations driven by time-evolving historical industrial and BMB aerosol emissions and aerosol-induced sea surface temperature (SST) anomalies, we identify two leading modes of multi-decadal aerosol optical depth (AOD) variability in boreal summer, together accounting for 94% of the AOD variance from 1930-2030. Mode 1 depicts a monotonic increase over low latitudes, while Mode 2 describes a sinusoidal trajectory over Northern Hemisphere continents with weaker opposite changes over South and East Asia. These AOD modes drive distinct atmospheric circulation, precipitation and terrestrial air temperature responses. We separate the atmospheric radiative and ocean-mediated pathways of response through a novel design using time-evolving aerosol-induced SST anomalies from the Community Earth System Model version 1 (CESM1) Single-Forcing and All-Forcing Large Ensembles. We find that ocean-mediated effects dominate the large-scale atmospheric circulation and precipitation responses, while atmospheric radiative effects induce robust regional impacts and modulate the ocean-mediated response in remote regions. Our results demonstrate that transient aerosol impacts reflect a dynamic balance between atmospheric radiative and ocean-mediated pathways. These highlight the importance of considering both spatial pattern and response pathway when assessing aerosol-driven climate variations.

SIGNIFICANCE STATEMENT

Aerosols from industrial activities and biomass burning have changed significantly over the 20th century. We conduct a novel set of climate model simulations to investigate how the changing spatial distribution of these aerosol emissions influenced historical climate via atmospheric and oceanic pathways. Using a pattern-based approach, we find that these aerosols influence global climate by modifying ocean surface temperatures, which in turn drive changes in global-scale atmospheric circulation, affecting precipitation and terrestrial air temperature. Aerosols' interaction with radiation in the atmosphere drives local and regional impacts and modulates oceanic-driven responses in remote regions. Our results highlight the importance of

File generated with AMS Word template 2.0

evolving aerosol patterns in shaping historical anthropogenic climate change and underscore the complexity of atmospheric and oceanic pathways governing the responses.

1. Introduction

Aerosols from anthropogenic sources are one of the dominant drivers of climate change over the industrial era (IPCC AR6, 2021). Aerosols from industrial sources have played a key role in shaping historical patterns of forced climate change in the atmosphere and ocean, with impacts on regional temperature and precipitation (e.g., Dong et al. 2024; Shi et al. 2022; Kang et al. 2021; Deser et al. 2020; Xie et al. 2013). For instance, Northern Hemisphere (NH) industrial aerosol emissions have been linked to the observed southward shift of the tropical Pacific and Atlantic rain belts in the late 20th century (Ming and Ramaswamy, 2011; Hwang et al., 2013; Hill et al., 2015; Allen et al., 2015). Aerosols from industrial sources, including those at lower latitudes, have also contributed to the weakening of South and East Asian Summer Monsoon circulations and the associated decrease in monsoon precipitation (Bollasina et al., 2011, 2014), as well as Sahel drought and subsequent recovery (Hua et al. 2019; Hirasawa et al., 2020). Industrial aerosol emissions have also been implicated in the recent weakening of the NH summertime atmospheric circulation, including the upper-level jet stream (Dong et al., 2022) and storm tracks (Kang et al., 2024; Chemke and Coumou, 2024). In addition, the historical NH mid-latitude aerosol increase has been suggested to delay the emergence of Arctic amplification until the past few decades (Mueller et al., 2018; England et al., 2021) while their reductions after the 1980s are linked to recent enhanced summer warming in western Europe (Schumacher et al., 2024; Roesch et al., 2025). Furthermore, industrial aerosol emissions, by modulating atmospheric radiation reaching the surface, have affected oceanic properties such as sea surface temperature (SST), sea surface salinity and heat content (Shi et al., 2023; Dong et al., 2024), which in turn influence ocean heat uptake and heat exchange between basins (Li et al., 2023), and have delayed the formation of the "North Atlantic Warming Hole" (Dagan et al., 2020).

Biomass burning (BMB) emissions, another major partially anthropogenic source of aerosols, have co-evolved with industrial emissions. However, the large-scale climatic impacts of BMB aerosols have received little attention until recently, due in part to incomplete inventories of historical BMB emissions (Hua et al., 2024) and BMB's relatively minor effect on the global mean energy balance (IPCC AR6, 2021). In addition, large uncertainties in BMB-driven aerosol-cloud interactions, and their dependence on aerosol types has hampered

File generated with AMS Word template 2.0

progress (IPCC AR6, 2021). The recent acceleration of human-related wildfire worldwide has prompted renewed scrutiny of the role of BMB emissions in anthropogenic climate change (Cunningham et al., 2024). In particular, it has been demonstrated that BMB emissions reduce time-mean total aerosol radiative forcing (Heyblom et al., 2023), partially mitigating the effect of industrial aerosol emissions on the strength of the Atlantic Meridional Overturning Circulation (AMOC; Allen et al., 2024; Liu et al., 2024) and accelerating externally-forced 20th century warming of the tropical Indian Ocean at a faster speed relative to other tropical ocean basins (Tian et al., 2023). In addition, interannual variations in BMB emissions have been shown to produce a sizeable effect on NH climate via non-linear aerosol-cloud interactions, contributing to high-latitude warming and Arctic sea ice decline in recent decades (Fasullo et al., 2022; DeRepentigny et al. 2022).

Industrial aerosol and BMB emissions are spatially heterogenous and have evolved substantially over time though with different spatiotemporal patterns. Industrial aerosol emissions are primarily located in the NH subtropics and middle latitudes, while BMB emissions mainly occur in the deep tropics and boreal regions (Van Der Werf et al., 2017). From the 1950s-1970s, industrial aerosol emissions increased rapidly over North America and western Europe, followed by marked declines resulting from clean air legislation (e.g., Deser et al., 2020). After the late 1970s, the locus of industrial aerosol emissions shifted to East Asia and South Asia. Following the passage of China's Air Pollution Prevention and Control Action Plan (Zhang et al., 2021), local industrial emissions dropped rapidly particularly after 2013 (Wang et al., 2021), shaping a dipole pattern between East and South Asia (Xiang et al., 2023). Meanwhile, tropical BMB emissions increased substantially over the second half of the 20th century in central Africa, South America and Southeast Asia due to agricultural activities and land use changes (Van Der Werf et al., 2017). Boreal BMB emissions have also risen over the 20th century, particularly in Siberia and parts of Canada (Van Der Werf et al., 2017).

The effect of radiative forcings such as aerosols can be decomposed into atmospheric radiative and ocean-mediated components. These are commonly referred to as "fast" and "slow" responses, respectively, reflecting the timescales over which they appear, where "fast" denotes the response in the absence of significant surface temperature changes and "slow" denotes the surface temperature feedback response (Gregory et al., 2004; Bala et al., 2009). Distinguishing them is important because their drivers emerge on different timescales, and thus the timescale of corresponding responses varies. This decomposition is typically assessed using

File generated with AMS Word template 2.0

a parallel set of idealized experiments in which aerosol emissions averaged over a particular time interval of interest are prescribed in both the fully-coupled model and its atmosphere-only component (e.g., Samset et al.,2016; Liu et al., 2018).

While such a "time-slice" approach serves as a valuable tool for studying the fundamental physical processes underlying the response to a fixed aerosol emission target, it becomes limited under transient conditions. Given the distinct spatial distributions and temporal evolutions of industrial and BMB aerosols, their varied aerosol types (primarily absorbing carbonous particles for BMB and predominantly scattering particles for industrial aerosols) and location-dependent efficacies (Persad and Caldeira 2018), it is crucial to account for their evolving trajectories when assessing their climate impacts. Under the transient framework, the separation between "fast" and "slow" responses becomes blurred. In particular, the response to time-evolving aerosol emissions in the absence of SST changes (e.g., the radiatively forced contribution) will include a "slow" component by virtue of the fact that aerosol emissions vary slowly through time. Thus, both the atmospheric radiative and ocean-mediated effects of aerosols must be considered on decadal and longer time scales. To date, the climate response to time-evolving patterns of historical industrial, and to a lesser extent BMB, aerosol emissions has been investigated using fully coupled models (e.g., Deser et al., 2020; Wang and Wen, 2022; Dong et al., 2024). While such studies highlight the importance of accounting for the full spatiotemporal evolution of aerosol emissions, they do not allow for insights into the relative contributions of atmospheric radiative *vs.* ocean-mediated components of response. Moreover, the role of BMB aerosols and their interplay with industrial aerosols has been largely ignored.

We address these gaps by employing a novel atmospheric modeling framework to decompose the combined effects of time-varying industrial and BMB aerosol emissions into atmospheric radiative and ocean-mediated components. Specifically, we conduct a suite of experiments with Community Atmosphere Model version 5 (CAM5) forced with time-varying historical aerosol (industrial plus BMB) emissions and associated SST responses individually and in combination, where the aerosol-induced SST changes are derived from the fully coupled CESM1 Single-Forcing and All-Forcing Large Ensembles (Kay et al., 2015; Deser et al., 2020). This approach allows us to elucidate the individual roles of evolving atmospheric radiative *vs.* ocean-mediated impacts of industrial and BMB aerosols on historical climate change. A similar methodology has been previously used in the context of idealized 1% per year CO_2 forcing (He and Soden, 2015) and quadrupling of CO_2 concentration (Tiffany and Vigot, 2015)

File generated with AMS Word template 2.0

experiments, but this is the first time it has been adopted for the historical evolution of industrial and BMB aerosols to the best of our knowledge. If adopted in a model intercomparison effort, this framework could also be beneficial for understanding models' structural diversity in aerosol-induced climate change. In addition, this protocol may prove useful for informing dynamical and statistical regional downscaling applications, as it provides large-scale, aerosol-forced signals that can serve as consistent boundary conditions. This consistency is particularly valuable for intercomparisons across models and methods, where isolating the aerosol influence on regional climate remains a key challenge (Nabat et al., 2025).

This study has three aims: 1) To identify the dominant patterns of time-varying aerosol emissions from industrial and BMB sources over the historical period (1920-present); 2) To assess how the dominant patterns of time-evolving aerosol emissions influence precipitation, terrestrial air temperature and the large-scale atmospheric circulation; and 3) To quantify the relative contributions of atmospheric radiative *vs.* ocean-mediated pathways of response. We focus on boreal summer (June-to-August, JJA), when NH monsoon systems and low-level jets drive strong signals, making it a natural season for assessing aerosol impacts particularly at regional scales. Our experimental design is described in Section 2, results are reported in Section 3, and summarized and discussed in Section 4.

2. Data and Methods

a. Model Simulations

We use CAM5 (Neale et al., 2010) coupled to Community Land Model version 4 (CLM4; Lawrence et al., 2011) at a spatial resolution of 1° for our AMIP simulations. CAM5 and CLM4 are the atmospheric and land model components of CESM1, respectively. CAM5 deploys a three-mode modal aerosol scheme (Liu et al., 2012) with prognostic aerosols and includes both the direct and indirect aerosol radiative effects for liquid and ice phase clouds (Morrison and Gettelman 2008). CLM4 includes a biogeochemical model which can prognostically simulate vegetation changes and a Snow and Ice Aerosol Radiation model which accounts for aerosol's impact on snow cover, as well as its radiative feedback.

We conducted three sets of AMIP ensembles, termed RAD-AMIP, SST-AMIP and FULL-AMIP (Table 1). Each set has 10 ensemble members and covers the period 1920-2030. For each set, the ensemble members are initialized with a small (order 10^{-14} K) random atmospheric temperature perturbation to create ensemble spread. RAD-AMIP uses time-varying CMIP5

File generated with AMS Word template 2.0

historical (prior to 2006) and Representative Concentration Pathway (RCP) 8.5 (2006 onward) industrial (AER_{indus}) and BMB (from agriculture activities, grass and forest fires) aerosol emissions (Lamarque et al., 2010). All other radiative forcings, as well as SSTs and sea ice concentrations (SICs), are set to their 1920 ensemble-mean seasonal cycles from the 40-member CESM1 "All Forcing" Large Ensemble (ALL). SST-AMIP uses time-varying aerosol-induced SSTs and SICs; all radiative forcings including AER_{indus} and BMB are set to their 1920 ensemble-mean seasonal cycles in ALL. The time-varying aerosol-induced SSTs and SICs are computed from the difference between the ensemble-mean of ALL and the sum of the ensemble-means of the fixed AER_{indus} and fixed BMB CESM1 Single Forcing Large Ensembles following Deser et al. (2020). FULL-AMIP uses the same time-varying aerosol emissions as RAD-AMIP plus the same time-varying SSTs and SICs as SST-AMIP. Given that the RAD-AMIP and SST-AMIP responses are largely additive (see below), we conclude that our AMIP experimental design is a valid approach for separating atmospheric radiative and ocean-mediated (SST-driven) components of the aerosol-forced response. Throughout the remainder of the manuscript, we refer to the SST-AMIP signal as the "ocean-mediated" or "SST-driven/induced" response and the RAD-AMIP signal as the "radiative forcing", "radiatively driven/induced/forced" or "atmospheric radiative" response.

Table 1. CAM5 AMIP experiments and their forcings. Each set of experiments contains 10 ensemble members and covers the period 1920-2030. See text for details.

	RAD-AMIP	**SST-AMIP**	**FULL-AMIP**
Radiative Forcing	Time-varying industrial and BMB aerosol emissions. All other radiative forcings fixed at 1920 levels.	All radiative forcings fixed at 1920 levels.	Time-varying industrial and BMB aerosol emissions. All other radiative forcings fixed at 1920 levels.
SST/SIC Forcing	SST and SIC fixed at 1920 levels.	Time-varying SST and SIC induced by industrial and BMB aerosol emissions.	Time-varying SST and SIC induced by industrial and BMB aerosol emissions.

b. AOD and SST patterns

File generated with AMS Word template 2.0

To define the dominant patterns of aerosol radiative forcing in FULL-AMIP, we apply Empirical Orthogonal Function (EOF) analysis to JJA AOD (550nm wavelength) based on low-pass filtered (using 10-year running means) ensemble means from 1930-2030 (similar results are obtained using AOD from RAD-AMIP which is not shown; we exclude 1920-1929 to minimize the influence of residual memory from ocean initial conditions). The two leading AOD modes account for 94% of AOD variance during 1930-2030 and are thus the focus of our analysis. To define the aerosol-induced SST patterns, we regress 10-year low-pass filtered ensemble mean SSTs in FULL-AMIP onto the normalized AOD Principal Component (PC) timeseries. Applying EOF analysis directly to the aerosol-induced SST field yields nearly identical patterns to those obtained via regression onto the AOD PCs, although there is a slight (3-4 year) phase lag between the SST PCs and their AOD PC counterparts (not shown). The atmospheric responses to the two leading AOD modes are obtained by regressing 10-year low-pass filtered ensemble means of precipitation, sea level pressure (SLP) and land surface air temperature (LSAT) in FULL-AMIP, RAD-AMIP and SST-AMIP onto the normalized AOD PCs. Substituting aerosol-induced SST PCs in place of AOD PCs yields similar atmospheric regression patterns (not shown); thus, for simplicity, we use the AOD PCs throughout this study. Statistical significance of all regression values is assessed using a two-tailed Student's t-test at the 95% confidence level.

3. Results

a. *Leading modes of AOD variability and associated SST patterns*

The two leading modes of JJA AOD variability show distinctive temporal and spatial characteristics (Fig. 1). PC1, which explains 56% of the AOD variance, depicts a pronounced (3 standard deviation) increase from the 1930s-1980s with little change thereafter, while PC2, which explains 38% of the AOD variance, shows more sinusoidal behavior, with a positive trend from about 1935-1975 followed by a steep decline to the early 2020s (Figs. 1a,d). The corresponding AOD spatial pattern associated with PC1 exhibits positive regression values over low latitudes of the Eastern Hemisphere, with regional hotspots in East and South Asia associated with industrial emissions and in tropical South Africa, South America, Indonesia and Malaysia associated with BMB emissions; weak negative values are found in the eastern US and western Europe (Fig. 1b). AOD Mode 2 depicts a zonally-asymmetric NH AOD pattern, with large positive values in the eastern US and western Europe juxtaposed against weaker negative values in South and East Asia from industrial aerosol emissions and in eastern

File generated with AMS Word template 2.0

Siberia from BMB emissions (Fig. 1e). Qualitatively, Mode 1 captures the rapid industrialization of Asia and Africa in the past century, along with the peak of major Asian aerosol emissions in the 2010s through present (Takemura et al., 2012). Mode 2 represents industrialization followed by clean air regulation in the Western Hemisphere.

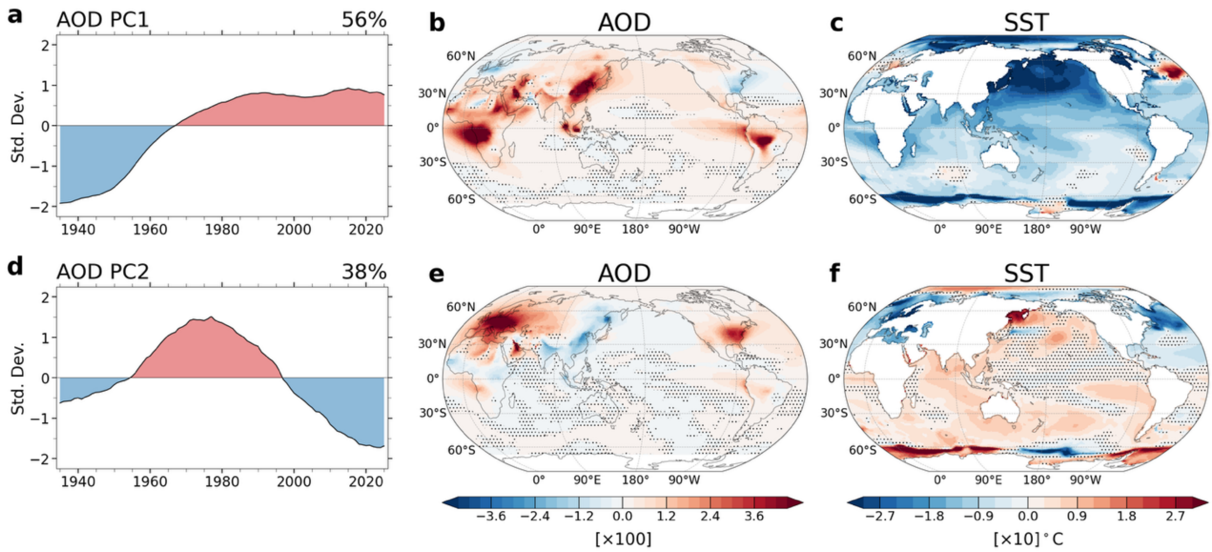

Figure 1. (a,d) Principal Component (PC) time series of Aerosol Optical Depth (AOD) in JJA based on FULL-AMIP. Percent variance explained by Modes 1 and 2 (PC1 and PC2) are given in the upper right. (b,c) Regression of JJA AOD (× 100) and SST (℃ × 10) in FULL-AMIP onto AOD PC1. (e,f) As in (b,c) but for AOD PC2. Regions without stippling are significant at the 95% confidence level based on a two-tailed Student's t-test.

The SST anomalies associated with AOD Mode 1, obtained by regressing ensemble-mean JJA SST anomalies from FULL-AMIP onto AOD PC1, exhibit widespread cooling, as expected from the global increase in AOD (Fig. 1c). The cooling is greatest over the North Pacific and along the sea ice margins of both hemispheres. A strong interhemispheric SST anomaly gradient is evident over the Pacific sector and to a lesser extent the Indian Ocean, likely associated with aerosol emissions over South and East Asia (Hwang et al., 2024). Pronounced SST warming is found in the central subpolar North Atlantic. This may be associated with a strengthening of AMOC and accompanying increase in northward ocean heat transport in response to AOD reductions over eastern North America and Europe (Cai et al., 2006; Delworth & Dixon, 2006; Booth et al., 2012; Menary et al., 2020; Dagan et al., 2020), but local wind-driven processes may also play a role.

The SST anomalies associated with AOD Mode 2 are generally weaker than those associated with Mode 1 and depict a strong zonal contrast over the NH with widespread cooling over the North Atlantic and Mediterranean and warming over most of the North Pacific (Fig. 1f). The North Atlantic cooling likely arises in response to increased aerosol emissions over the eastern US and Europe (e.g., Undorf et al., 2018a), while the warming in the Pacific and Indian Ocean sectors is presumably a result of reduced AOD over eastern Asia and India (Fig. 1f).

Investigation of the mechanisms underlying the SST patterns associated with each AOD Mode is beyond the scope of this study, but related analyses may be found in Kang et al. (2021), Shi et al. (2023), Hwang et al. (2024) and Diao et al. (2025), although none considered the combined effects of industrial and BMB aerosols. Here, our interest is in how these aerosol-induced SST patterns impact the atmosphere.

b. Global atmospheric response patterns

We begin by examining the global atmospheric response to combined atmospheric radiative and SST-driven changes associated with each AOD mode. To do this, we regress the FULL-AMIP JJA ensemble-means onto the PC timeseries associated with each AOD Mode. Regression maps of precipitation, SLP and LSAT for AOD Mode 1 are shown in Fig. 2 and for AOD Mode 2 in Fig. 3. Regression maps for associated surface downward short-wave radiative flux (SWSD) under total-sky, clear-sky and cloudy-sky conditions in both modes are given in Fig. 4.

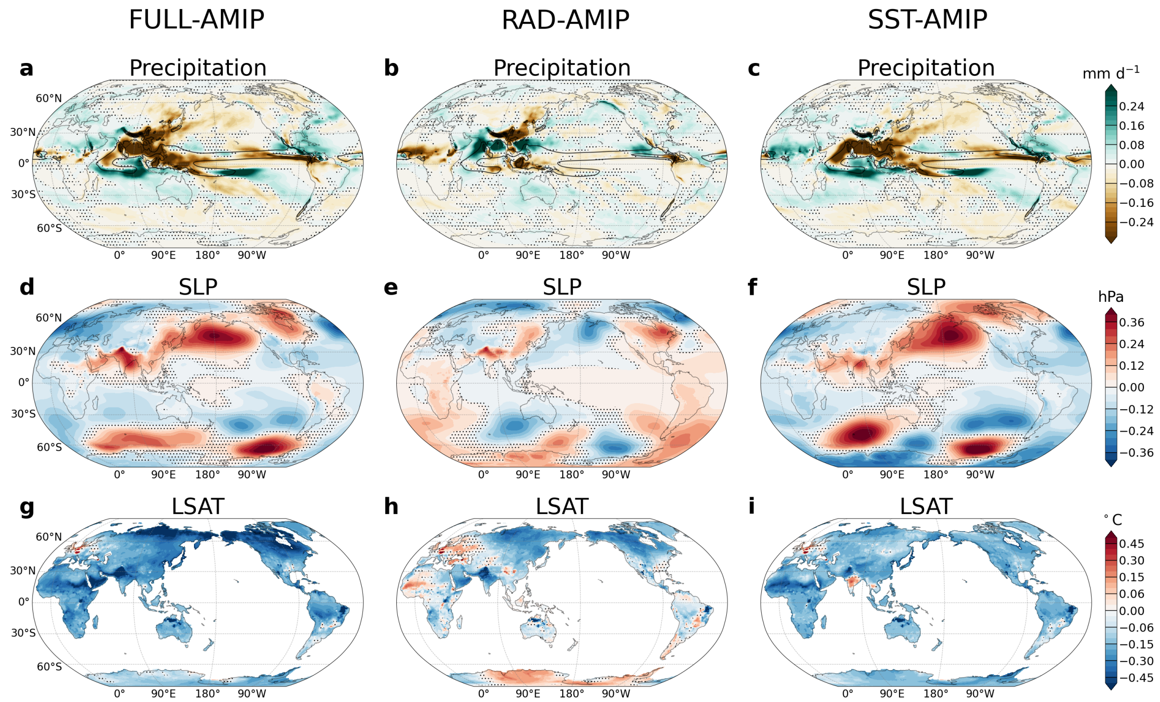

Figure 2. AOD Mode 1 response of (a,b,c) precipitation (mm d^{-1}), (d,e,f) sea level pressure (SLP; hPa) and (g,h,i) land surface air temperature (LSAT; °C) in FULL-AMIP, RAD-AMIP and SST-AMIP regressed onto AOD PC1. Regions without stippling are significant at the 95% confidence level based on a two-tailed Student's t-test. Black contours on precipitation panels show the climatological 6 mm d^{-1} isopleth.

File generated with AMS Word template 2.0

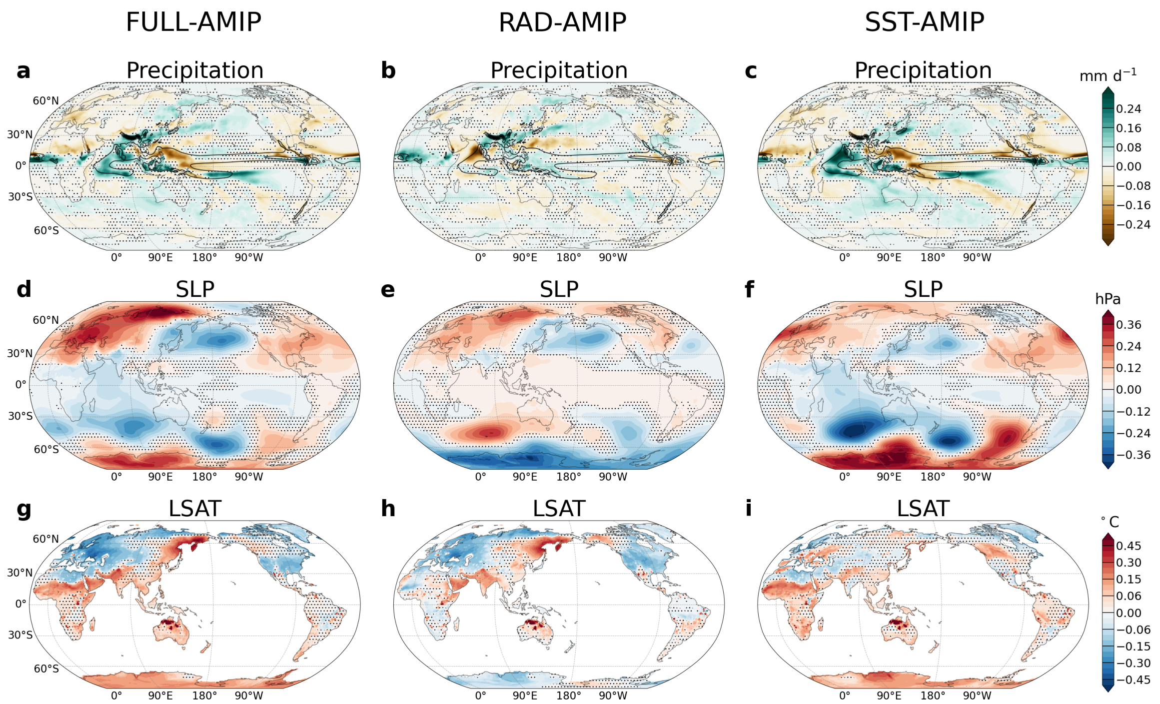

Figure 3. As in Figure 2 but for AOD PC2.

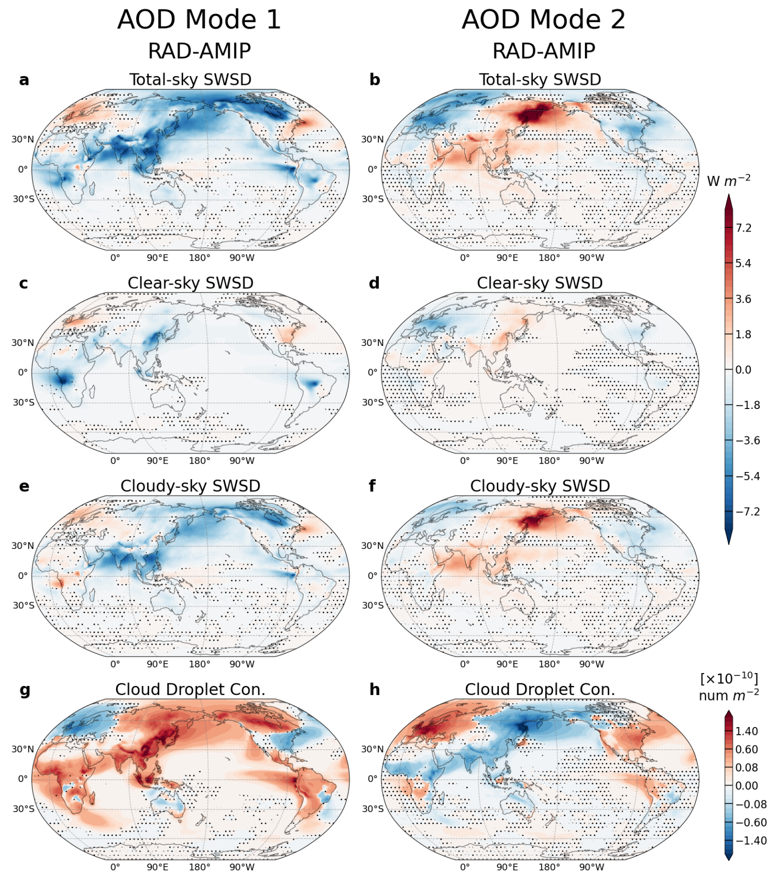

Figure 4. AOD Mode 1 and Mode 2 responses of short-wave surface downward (SWSD) radiative flux (W m^{-2}) under (a,b) total-sky, (c,d) clear-sky and (e,f) cloudy-sky conditions, and (g,h) vertically integrated cloud droplet number concentration (num $m^{-2} \times 10^{-10}$) in RAD-AMIP regressed onto (left) AOD PC1 and (right) AOD PC2. Regions without stippling are significant at the 95% confidence level based on a two-tailed Student's t-test.

File generated with AMS Word template 2.0

Both modes exhibit statistically significant responses that are global in scale. AOD Mode 1 features prominent drying over South and East Asia, the northern Indian Ocean and the Maritime Continent, regions proximate to the main centers of AOD increase (Fig. 2a), accompanied by reduction in SWSD (Fig. 4a). Compensating areas of wetting occur directly south of the equator in the Indian Ocean and central Pacific. At higher latitudes, widespread drying is found over the Southern Ocean, the North Pacific, northeastern Asia and western North America, while wetting occurs over the subtropical south Indian and southeast Pacific Oceans, tropical Africa, southern Europe, the Caribbean and parts of the North Atlantic. Areas of drying (wetting) generally correspond to anticyclonic (cyclonic) SLP anomalies, with largest SLP magnitudes in the extra-tropics (Fig. 2d). The prominent positive SLP response over the North Pacific may be due to in part to a remote Rossby wave teleconnection excited by precipitation reductions over the northern Indian Ocean and Southeast Asia (Smith et al., 2016; Dittus et al., 2021) in addition to local SST cooling. The circulation response in other regions is discussed in Section 3c. AOD Mode 1 exhibits widespread terrestrial cooling (Fig. 2g), as expected from the global-scale increase in AOD (Figs. 1a,b) with widespread SWSD reductions (Fig.4a). The strongest cooling is found in boreal regions, likely associated with positive ice/snow albedo feedback. A "cooling hole" is seen over far western Europe, reflecting the local decrease in AOD with positive SWSD values (Fig. 4a). SWSD in FULL-AMIP closely resembles that in RAD-AMIP, whereas SST-driven SWSD responses primarily associated with cloud changes are much weaker. Cloud responses to aerosol strongly affect the SWSD response in remote regions (Fig. 4e), whereas the direct radiative effect dominates locally (Fig. 4c).

AOD Mode 2 shows generally weaker responses compared to Mode 1, especially for precipitation and LSAT (Fig. 3). Like Mode 1, Mode 2 AOD increases are generally accompanied by local terrestrial drying and cooling (Figs. 1e and 3g). For example, AOD increases over Europe and the eastern US are accompanied by negative SWSD, primarily driven by aerosol-cloud interactions, whereas AOD decreases over eastern Asia and India produce the opposite response (Figs. 4b,f,h). Remote precipitation responses are also evident, most prominently in the tropics, including a zonal dipole pattern of drying over the far western Pacific and wetting over the central Indian Ocean, and an increase in precipitation across the equatorial Atlantic. The large-scale SLP response over the extratropical NH is generally opposite in sign between Modes 1 and 2, in keeping with their contrasting NH AOD signatures

File generated with AMS Word template 2.0

(Figs. 2d, 3d and 4a,b). However, the tropical and SH SLP response patterns are distinctive between the two AOD modes.

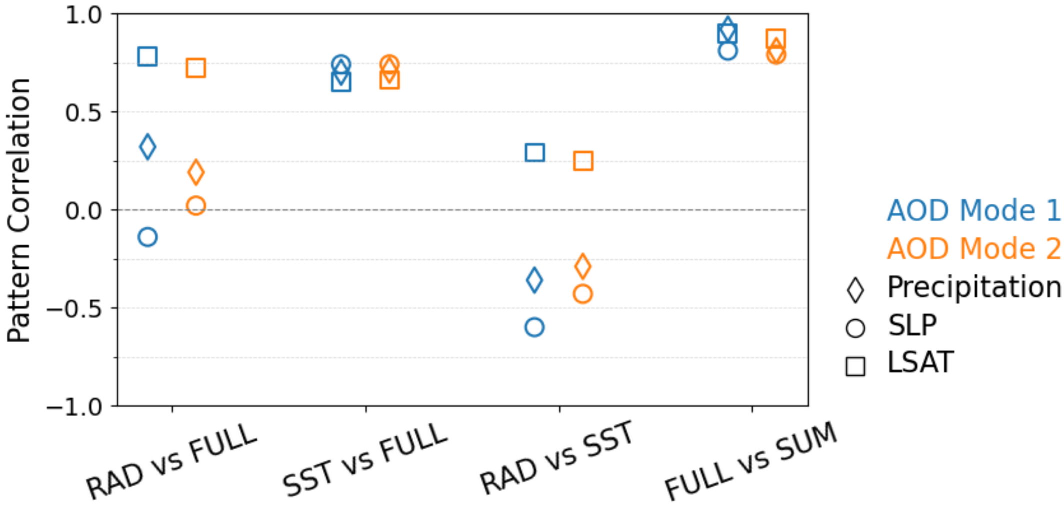

Figure 5. Global pattern correlations of precipitation (diamond), SLP (circle) and LSAT (square) regression maps associated with AOD Mode 1 (blue) and 2 (orange) between different pairs of AMIP simulations. SUM refers to the sum of RAD-AMIP (RAD) and SST-AMIP (SST) regressions. FULL refers to FULL-AMIP.

Next, we assess the relative contributions of atmospheric radiative and ocean-mediated pathways to the atmospheric responses in FULL-AMIP by regressing ensemble-mean fields from RAD-AMIP and SST-AMIP onto the AOD PCs. The two pathways produce distinctive and statistically significant global-scale atmospheric responses (Figs. 2 and 3). Comparing to FULL-AMIP, it is readily apparent that the SST-driven response dominates the large-scale patterns of precipitation and SLP response, while radiative forcing tends to oppose SST-induced responses, although the degree of compensation varies with region. On the other hand, radiatively forced and SST-driven responses make comparable contributions to the LSAT response in FULL-AMIP. Quantitatively, the leading role of the SST-induced response for the precipitation and SLP responses is evidenced by the high pattern correlations (exceeding 0.70) between SST-AMIP and FULL-AMIP, while those between RAD-AMIP and FULL-AMIP are substantially lower (< 0.33; Fig. 5). In contrast, the importance of both radiative forcing and ocean-mediated effect to the patterns of LSAT response is reflected in the comparable magnitudes of spatial correlation between RAD-AMIP and FULL-AMIP and between SST-AMIP and FULL-AMIP (around 0.65 and around 0.75, respectively; Fig. 5). Radiative forcing partially counteracts the SST-driven response for both precipitation and SLP responses, as seen by the modest negative pattern correlations between RAD-AMIP and SST-AMIP (Fig. 5). This negative correlation is particularly pronounced for the SLP response to AOD Mode 1 (-0.60),

File generated with AMS Word template 2.0

as is also visually apparent (Figs. 2e,f). However, for LSAT, the correlations between RAD-AMIP and SST-AMIP are weakly positive (Fig. 5).

As mentioned above, the interplay between atmospheric radiative and ocean-mediated pathways depends on the region and quantity of interest. In emission source regions such as East Asia, precipitation responses in both AOD modes are primarily driven by radiative forcing: in Mode 1, AOD increases induce local drying, while AOD decreases in Mode 2 induce local wetting (Figs. 1a,d, 2b and 3b). In contrast, the sign of South Asian precipitation response does not always align with local AOD changes because the SST-driven response dominates. For example, in AOD Mode 1, radiative forcing drives a wetting response despite positive AOD values over South Asia, and this radiatively forced wetting is largely offset by SST-driven drying (Figs. 1a and 2b,c). In the NH mid-latitude, the eastern North America and Europe exhibit robust precipitation and LSAT responses in both modes, driven by a combination of radiatively induced and SST-driven thermodynamic and dynamic mechanisms from local and remote forcing sources (Figs. 2b,c and 3b,c). In these regions, in both modes, LSAT changes reflect compensation between radiatively forced and SST-driven responses, whereas western European precipitation results from the reinforcement of the two pathways of response. Over North America, radiatively and SST-driven precipitation and LSAT responses exhibit distinct patterns, reflecting a tug-of-war between locally and remotely induced circulation influences by each pathway. For example, in AOD Mode 1, a radiatively driven negative North Atlantic Oscillation (NAO)–like response (a cyclonic system in the North Pacific) is opposed by SST-driven positive NAO-like response (an anti-cyclonic system in North Pacific). Whether these large-scale circulation responses are triggered by local or remote forcing is hard to determine, warranting further analysis.

In low-emission regions, such as the Sahel, for both modes, radiatively forced and SST-driven responses cancel each other, resulting in muted precipitation responses (Figs. 2b,c and 3b,c). For AOD Mode 2, radiatively induced and SST-driven SLP responses are of the same sign over most of the NH and tropics but of opposite polarity over the SH high latitudes (Figs. 3e,f). The NH LSAT response to AOD Mode 1 shows like-signed contributions from radiatively forced and SST-driven responses (Figs. 2h,i), whereas the LSAT response to AOD Mode 2 depicts nearly orthogonal patterns (Figs. 3h,i).

The complex regional interplay between radiatively forced and SST-driven responses would naturally raise a question of to what extent these responses are additive. We address this

File generated with AMS Word template 2.0

question by comparing the sum of the RAD-AMIP and SST-AMIP regressions (SUM) with the FULL-AMIP regressions. Both AOD modes show a large degree of additivity, as evidenced by the overall similarity in pattern and amplitude between SUM and FULL-AMIP (Fig. 6 for Mode 1 and Fig. S1 for Mode 2). In general, the differences between SUM and FULL-AMIP are relatively small in magnitude, albeit statistically significant, except for SLP at high latitudes where larger discrepancies are found. Pattern correlations between SUM and FULL-AMIP are high (0.79–0.92) for all three variables in both AOD modes (Fig.5).

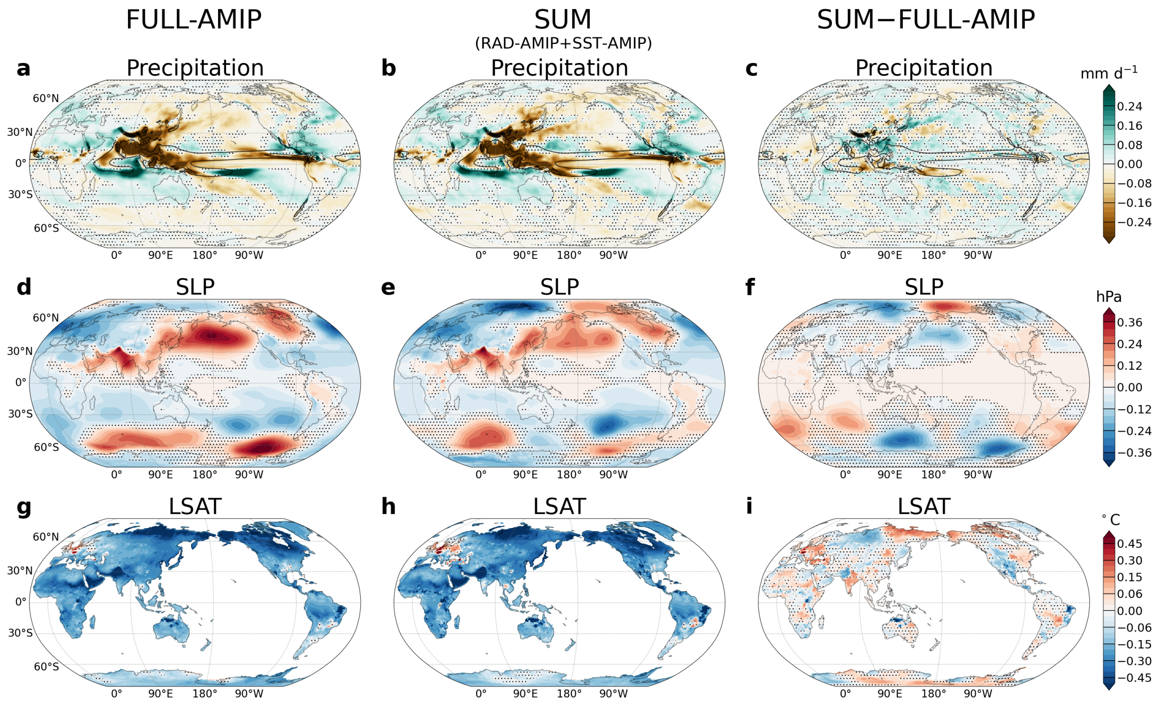

Figure 6. As in Fig. 2 but for additivity analysis based on AOD Mode 1 (a,d,g) FULL-AMIP, (b,e,h) the sum of RAD-AMIP and SST-AMIP (SUM), and (c,f,i) the difference of SUM and FULL-AMIP. Regions without stippling are significant at the 95% confidence level based on a two-tailed Student's t-test. Black contours on precipitation panels show the climatological 6 mm d^{-1} isopleth.

c. *Regional atmospheric response patterns*

The diversity of regional features described above makes it difficult to generalize the relative contribution of atmospheric radiative *vs.* ocean-mediated pathway on aerosol-driven atmospheric responses at the regional scale. To further illustrate this regional variation, we focus here on two areas: the tropical Indo-Pacific sector and Southern Ocean, characterized by distinct response patterns, to demonstrate how radiative forcing originating from regional AOD changes interacts with the SST-driven response to influence the atmosphere locally and remotely.

1) *Tropical Indian-Western Pacific sector*

File generated with AMS Word template 2.0

The pattern of precipitation response to AOD Mode 1 features a distinctive meridional dipole over the tropical Indian-Western Pacific sector in FULL-AMIP (Fig. 7a), indicative of an Asian Summer Monsoon response to shifting historical aerosol emissions that has been a topic of great interest in the literature (Bollasina et al., 2011; Persad et al., 2017; Undorf et al., 2018b; Westervelt et al., 2020). In our simulations, this precipitation dipole response corresponds to a cross-equatorial overturning circulation, with northerly wind anomalies at low-levels and southerly wind anomalies at upper-levels, which feeds anomalous upward motion along 5°-10°S accompanied by anomalous downward motion along 5°-15°N (Figs. 7a,b). This cross-equatorial overturning circulation response results from a subtle interplay between radiatively forced and SST-driven response, which impart different meridional scales and polarities of response. The radiatively forced response exhibits a narrow meridional dipole between the Asian subcontinent from the Tibetan Plateau eastward (27°-30°N) and the northern Indian Ocean-West Pacific (14°-23°N; Figs. 7c,d), while the SST-driven response displays a broader latitudinal dipole structure between the northern (5°-20°N) and southern (5°-12°S) portions of the Indian Ocean (Figs. 7e,f). The radiatively forced and SST-driven responses are offsetting over the northern Indian Ocean. As a result, the response in FULL-AMIP shows a hybrid structure, with characteristics of both the SST-driven response (i.e., the broad cross-equatorial dipole, albeit substantially weaker in its northern lobe) and the radiatively forced response (i.e., the narrow meridional dipole over the Tibetan Plateau extending eastward).

The SST-driven precipitation dipole response (Figs. 2a, 7a) likely results from the enhanced meridional temperature gradient over the Indian Ocean (i.e., stronger cooling north of the equator than south; Li et al., 2020), although the pronounced large-scale cooling of the North Pacific may also play a role in displacing the rain belt southward (recall Fig. 1c). Conversely, the radiatively forced precipitation dipole response is likely driven by locally induced drying and subsidence from aerosol emissions over East Asia, with compensating upward motion over the Arabian Sea, Bay of Bengal and the South China Sea (Bollasina et al., 2011; Persad et al., 2017; Westervelt et al., 2020); enhanced cooling over land may also contribute to ascent over the nearby seas.

Both aerosol direct and indirect radiative effects contribute to enhanced cooling over Southeast Asia in RAD-AMIP, as seen from the SWSD under clear and cloudy skies, respectively (Figs. 4a,c,e). Aerosol direct effects (e.g., clear-sky SWSD) dominate locally over the aerosol emission source regions (Fig. 4c), while aerosol indirect effects (e.g., cloudy-sky

File generated with AMS Word template 2.0

SWSD and associated increase in cloud droplet number concentration) prevail in adjacent regions including the northern Indian Ocean (Figs. 4e,g). Note that the reduction in cloudy-sky SWSD over the northern Indian Ocean and western North Pacific in RAD-AMIP would act to cool the underlying SSTs if the ocean were allowed to respond, consistent with the negative SST anomalies found in SST-AMIP. In SST-AMIP, adiabatic heating associated with the descending branch of the overturning circulation response over the northern Indian Ocean (Figs. 7e,f) reduces cloud cover and allows more insolation to reach the surface (not shown), warming the adjacent Indian Peninsula and parts of central Mainland Southeast Asia (Fig. 2i). However, this warming effect is overwhelmed by radiatively forced cooling (Fig. 2h), resulting in net cooling over these regions in FULL-AMIP (Fig. 2g).

The relative role of RAD-AMIP (i.e. atmosphere radiative effects) and SST-AMIP (i.e. ocean-mediated effects) provides valuable insight on the relative importance of in-situ *vs.* large scale responses to aerosol changes in driving summertime rainfall trends in this region, which has been a topic of substantial debate (Bollasina et al., 2011; Persad et al. 2017; Dong et al;, 2019; Li et al., 2018; Wang et al., 2019; Westervelt et al. 2020). AOD Mode 1 captures prevailing northly wind anomalies and precipitation reductions over Asian Summer Monsoon land regions, indicating the weakening of Asian Summer Monsoon (Li et al., 2018; Wang et al., 2019). The SST-driven cross-equatorial dipole circulation accounts for the precipitation response over the central to southern Indian Peninsula and adjacent oceans. Meanwhile East Asian Monsoon weakening arises primarily from radiatively dominated in-situ responses, including subsidence, land cooling and positive SLP anomalies, that suppress ascending motion particularly over the Tibetan Plateau extending eastward. These results suggest that historical South Asian Summer Monsoon weakening reflect effects of East Asian aerosols (Shawki et al, 2018) in Mode 1 here, given the importance of ocean-mediated response. But, when not decomposed by mode, the full response of South Asian Summer Monsoon to aerosols likely includes the contribution from other remote sources such as Europe and North America (Bollasina et al., 2014; Undorf et al., 2018b). In contrast to South Asian Summer Monsoon dominated by remote aerosols, East Asian Monsoon weakening is primarily attributable to local aerosols through atmospheric radiative pathway. Given that the total response of East Asian Summer Monsoon precipitation to aerosols is dominated by Mode 1 (not shown), which is compensated by weak precipitation increase in response to negative local AOD values in Mode 2 (Figs. 1d and 3a), this indicates that historical East Asian Summer Monsoon weaking and

File generated with AMS Word template 2.0

associated land drying is likely dominated by local aerosols through the atmospheric radiative pathway.

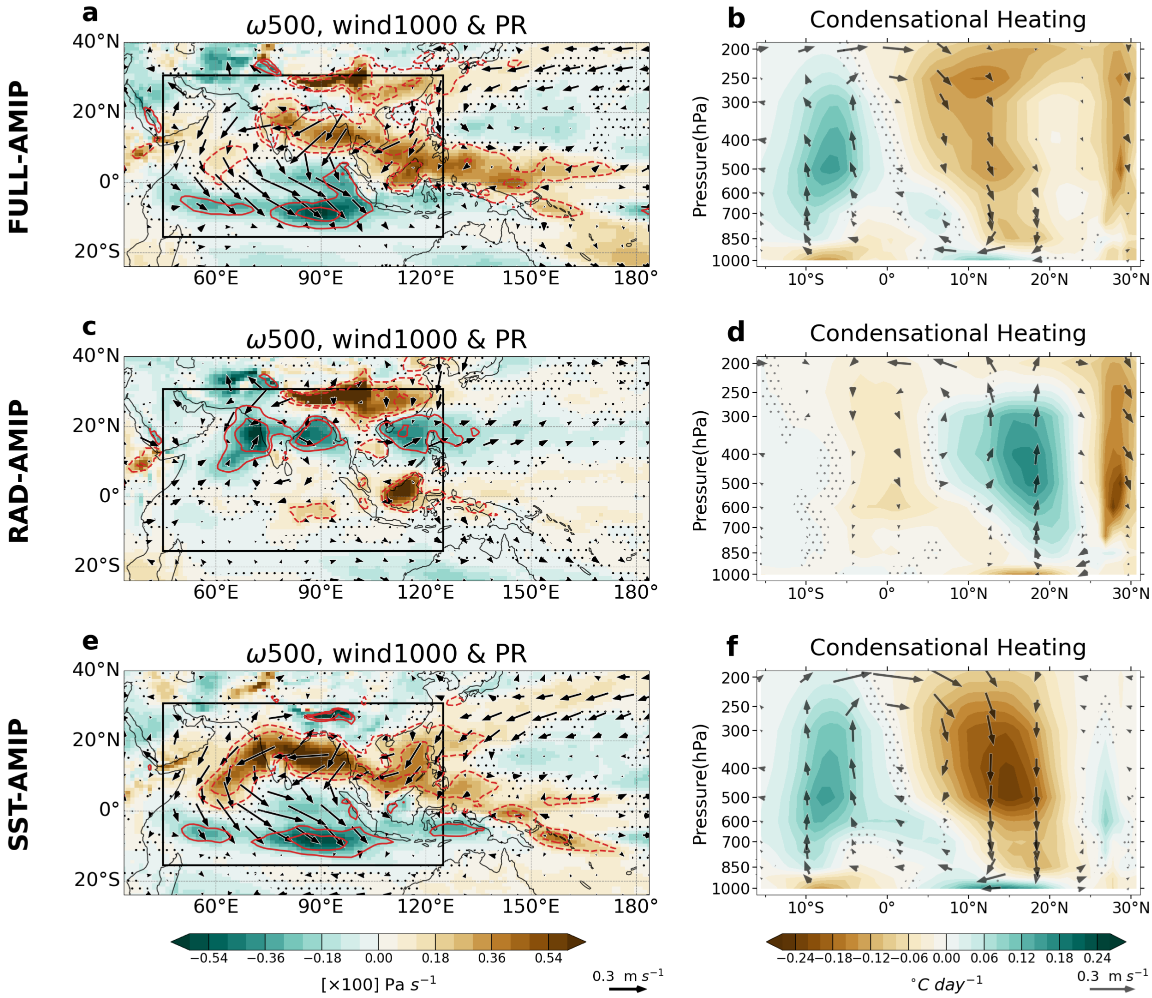

Figure 7. AOD Mode 1 tropical Indo-Pacific response of (a,c,e) 500hPa ω ($Pa\ s^{-1} \times 100$; color shading), 1000 hPa vector wind (m s^{-1}; reference vector in lower right) and precipitation (mm day^{-1}; red contours), and (b,d,f) zonally-averaged (45°-125°E) condensational heating (℃ d^{-1}; color shading) and v, ω vectors (v: m s^{-1}, reference vector in lower right; ω: $Pa\ s^{-1} \times 50$) in FULL-AMIP, RAD-AMIP and SST-AMIP regressed onto AOD PC1. Red contours in (a,c,e) show precipitation regression slopes, starting from ±0.2 mm d^{-1} and contoured at ±0.2 mm day^{-1} intervals, with solid lines for positive values and dashed lines for negative values. Region for the zonally-averaged cross section is outlined in (a,c,e). Areas without stippling are significant at the 95% confidence level based on a two-tailed Student's t-test. Horizontal wind magnitudes < 0.01 m s^{-1} are omitted for clarity.

2) Southern Hemisphere Circulation

A notable aspect of AOD Mode 1 is the SLP response pattern over the SH, which resembles a Rossby wave train in both RAD-AMIP and SST-AMIP, but with opposite sign (Figs. 2e,f). In contrast, FULL-AMIP shows a zonally symmetric structure over the SH extra tropics, with positive (negative) SLP anomalies at high (middle) latitudes (Fig. 2d). SH circulation trends have been linked to anomalous heating in the tropics which can trigger tropical–extratropical teleconnections (Berbery et al. 1992; Hoskins and Ambrizzi 1993). Guided by this theory, we pose an open question: can low-latitude aerosols, particularly central African biomass burning emissions given their geographic proximity, modulate SH circulation through teleconnection dynamics via an atmospheric radiative pathway, and how does this compare with teleconnections driven by the ocean-mediated response? These SH anomalous upper-level circulations can potentially influence Australian precipitation (Ashok et al., 2003; Cai et al., 2011) and Antarctic climate through the Tropical-Antarctic teleconnection (Ding and Steig, 2013; Li et al., 2021).

To understand the origin of the Rossby wave train responses, we examine the upper-level circulation and its connection to tropical precipitation. The 250 hPa meridional wind (V250) anomalies clearly delineate poleward propagating Rossby wave trains of opposite sign in response to the radiatively forced and SST-driven responses, which appear to originate in the Gulf of Guinea and propagate southeastward over the southern Indian Ocean and into the Pacific sector of the Southern Ocean (Figs. 8c,e). The SST-driven Rossby wave train takes a slightly more poleward route than the radiatively forced one. FULL-AMIP lacks a poleward-propagating Rossby wave signature due to the large degree of cancellation between RAD- and SST-AMIP (Fig. 8a). Instead, FULL-AMIP shows a zonally-oriented V250 wave train emanating from the tip of South Africa and extending eastward across the Indian and Pacific Oceans along the latitude (30°S) of the subtropical jet maximum, which acts as a wave guide (Fig. 8b).

Both the radiatively forced and SST-driven V250 Rossby wave trains appear to be initiated by tropical precipitation and associated diabatic heating anomalies over Africa and the Indian Ocean (Figs. 8d,f). In SST-AMIP, upper-level divergence associated with increased precipitation over the Sahel produces the negative (northerly) V250 anomaly centered over the Gulf of Guinea (Fig. 8f). As the anomalous northerly divergent winds cross the equatorward flank of the climatological subtropical westerly jet, it generates a negative Rossby wave source (RWS) to the west of South Africa, which triggers a downstream Rossby Wave response (Fig. 8f). Increased precipitation in the tropical Indian Ocean along 10°S may also act to reinforce the Rossby Wave response. These results are consistent with previous studies which show the critical role of the subtropical jet in amplifying upper-level circulation anomalies emanating from tropical heating (Berbery et al. 1992; Hoskins and Ambrizzi 1993; Li et al., 2015) and serving as a waveguide into the SH extra tropics (Gillett et al. 2021). In RAD-AMIP, upper-

File generated with AMS Word template 2.0

level convergence associated with diminished precipitation over the Sahel produces the positive (southerly) V250 anomaly centered over the Gulf of Guinea (Fig. 8d). Unlike SST-AMIP however, RAD-AMIP shows a large AOD increase over the African Democratic Republic associated with local BMB emissions (recall Fig. 1b). The resulting anomalous heat source from absorbing BMB aerosols is balanced by adiabatic ascent, accompanied by upper-level divergence (Fig. 8d). The divergent V250 anomaly crossing the equatorward flank of the subtropical jet over the southwestern Indian Ocean generates a positive RWS anomaly, which in turn triggers the downstream Rossby wave train response (Fig. 8d).

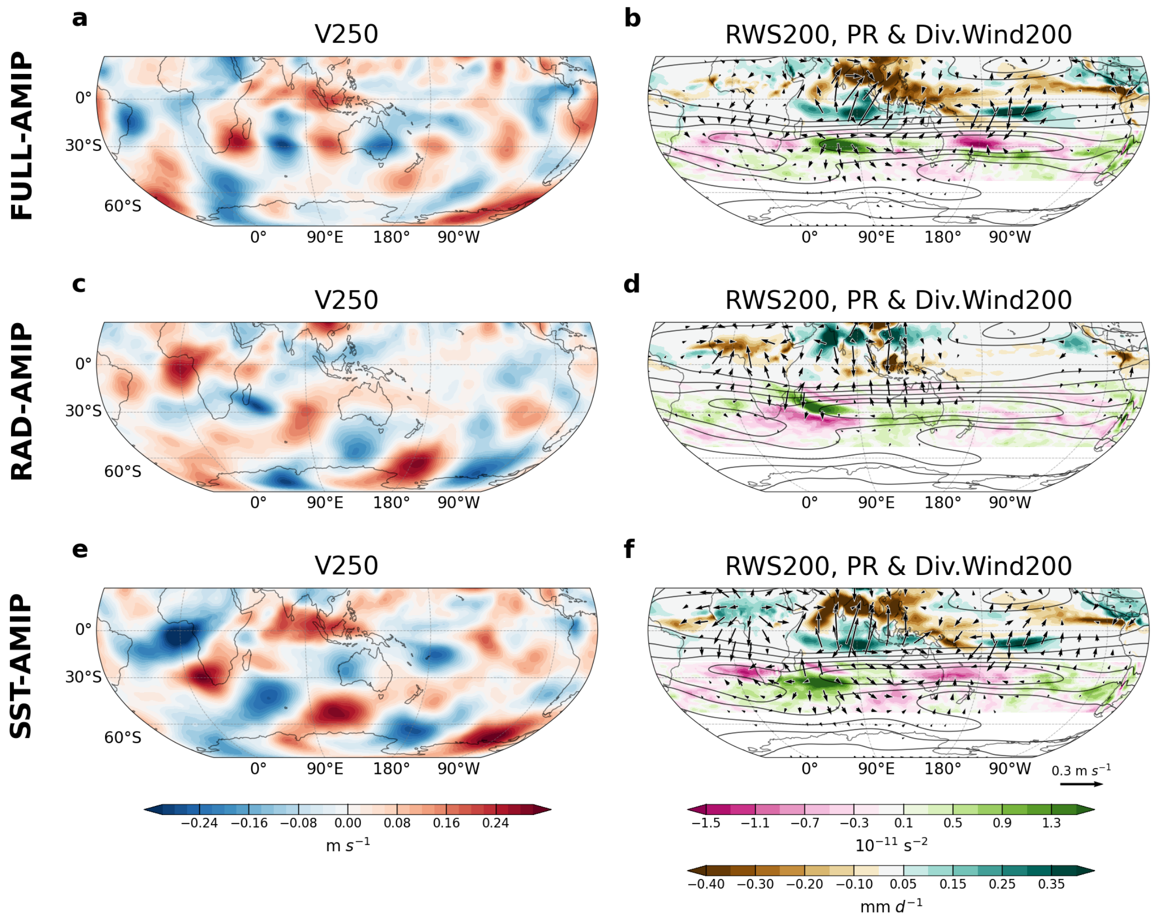

Figure 8. AOD Mode 1 Southern Hemisphere response of (a,c,e) 250 hPa meridional wind (V250; m s^{-1}) and (b,d,f) 200 hPa Rossby wave source (RWS200; pink-green color bar; 10^{-11} s^{-2}), precipitation (PR; green-brown color bar; mm d^{-1}) and 200 hPa divergent wind vector (m s^{-1}; reference vector in lower right) regressed onto AOD PC1 in FULL-AMIP, RAD-AMIP and SST-AMIP. For clarity, RWS200 (precipitation) regressions are only shown in the latitude band 52°-20°S (19°S-26°N) in FULL-AMIP and SST-AMIP and 52°-6°S (6°S-26°N) in RAD-AMIP; wind vectors with magnitudes $<$ 0.03 m s^{-1} are omitted. The climatological 250hPa zonal wind is contoured in black (contour interval = 10 m s^{-1} from 5-45 m s^{-1}).

Due to the largely canceling Rossby wave trains, the SH SLP response in FULL-AMIP shows a more zonally symmetric structure than either RAD-AMIP or SST-AMIP (recall Figs. 2d-f). We do not have a definitive explanation for this pattern of response, other than to

File generated with AMS Word template 2.0

conjecture that it may be linked to the zonally-symmetric precipitation response in the deep tropics over the Indian and Pacific sectors, and to note that it stems from a subtle balance between radiatively and SST-driven effects, which are not entirely additive (recall Fig. 6).

The opposing Rossby-wave-like signatures in RAD- and SST-AMIP and their tropical origins suggest a plausible teleconnection pathway by which low-latitude aerosols can influence SH circulation through anomalies in tropical convection. In RAD-AMIP, the response originates from divergent flow associated with adiabatic ascent induced by absorbing African aerosols and Sahel drying, together with precipitation anomalies over the tropical Indian Ocean, whereas in SST-AMIP it arises primarily from diabatic heating associated African convection. Despite originating from different processes, both pathways generate poleward-propagating Rossby wave trains of opposite sign. Their near cancellation, along with the relatively weak influence of Sahel precipitation anomalies featuring a meridional dipole pattern, may help explain the muted, zonally symmetric SH signal in FULL-AMIP. We reiterate that this is a working hypothesis, and firm attribution requires further verification such as using barotropic linear model experiments forced with the anomalous heating or divergent flow from our simulations to test whether similar wave train responses can be reproduced.

4. Summary and Discussion

There is increasing recognition that the global climate response to anthropogenic aerosols is sensitive to the pattern of regional emissions, which has shifted over time, necessitating a broader view of their role in historical climate change (Persad and Caldeira, 2018; Deser et al. 2020; Kang et al. 2021; Wang and Wen, 2022; Persad, 2023; Shi et al. 2023; Dong et al. 2024; Diao et al. 2025). In particular, two distinct modes of AOD variability from industrial sources have been identified over the past century: the “global increase mode” primarily associated with Asian emissions but modulated by emissions over North America and Europe, and the “shift mode” reflecting a zonal redistribution of NH emissions between the western and eastern hemispheres (Kang et al. 2021; Wang and Wen, 2022; Shi et al. 2023; Dong et al. 2024). These AOD modes can produce synergistic and competing effects with GHGs depending on the period of interest, complicating detection and attribution efforts (Dong et al. 2024). The dynamical mechanisms underpinning the global response to the “global increase” and “shift” modes of industrial aerosol emissions have been investigated in idealized coupled modeling studies, revealing the importance of both atmospheric and oceanic processes (Kang et al. 2021; Wang and Wen, 2022; Shi et al. 2023; Diao et al. 2025). However, non-linear interactions

File generated with AMS Word template 2.0

between aerosol emissions in different regions complicates a full understanding and interpretation of the combined effects of the two AOD modes (Diao et al. 2025).

In this study, we provide additional insight into the pathways by which time-evolving anthropogenic aerosols from combined industrial and BMB sources over the past century influence boreal summer (JJA) climate. In particular, we utilize a novel atmospheric modeling framework to separate the atmospheric radiative and ocean-mediated pathways of response. We decompose the full spatio-temporal evolution of historical aerosol emissions into two leading modes and elucidate the response pathways for each mode.

AOD variations arising from industrial and BMB sources can be decomposed into two leading modes, which together explain 94% of global JJA AOD variance during 1930-2030 (56% for Mode 1 and 38% for Mode 2). AOD Mode 1 increases monotonically over the first half of the record with little change thereafter, in contrast to Mode 2 which exhibits sinusoidal behavior, with a positive trend from the mid-1930s to the mid-1970s followed by a steep decline to the early 2020s. Mode 1 features positive AOD anomalies at low latitudes, with regional hotspots in East and South Asia associated with industrial emissions and in tropical South Africa, South America, Indonesia and Malaysia associated with BMB emissions, accompanied by weak negative AOD anomalies in western Europe and the eastern US. While Mode 2 is characterized by large positive AOD values in western Europe and the eastern US, juxtaposed against weaker negative values in South and East Asia and eastern Siberia. The two AOD modes are broadly consistent with the "global increase" and "shift" modes reported in prior studies that considered industrial aerosols alone (e.g., Wen and Wang, 2022; Shi et al., 2023; Dong et al., 2024).

By spanning through 2030, our results provide additional insight on historical and near-present aerosol variability. Our simulations use RCP8.5 aerosol emission trajectory from 2006 onward, which projects a peak of Asian aerosol emissions in the 2010s, followed by a decline in the 2020s-2030s, due to decreasing emissions in Japan offset by increases in other Asian regions (including China; see Fig.6b in Takemura et al., 2012). In contrast, CMIP6 shows higher AOD in China than CMIP5 prior to 2006 (see Fig. 2a in Wang et al., 2014) and also fails to capture China's AOD decline from 2006 to 2014 (Wang et al., 2021). Meanwhile, in the recent Shared Socioeconomic Pathway (SSP) future scenarios, SSP 3-7.0, which is comparable to RCP 8.5 in terms of the greenhouse gas trajectory, projects China's aerosol emissions increase through the 2050s (see Fig.2 in Lund et al., 2019). Therefore, though

File generated with AMS Word template 2.0

imperfect, the middle-of-road aerosol emission trajectory of RCP 8.5 more closely resembles Asian aerosol emission conditions from 2006 to present compared to the latest CMIP6 and SSPs, and the resulting global and regional AOD estimates remain within the observational error range (IPCC AR6; Lund et al., 2019; Takemura et al., 2012; Wang et al., 2024).

In AOD Mode1, the shift of PC1 from a positive slope to a negative slope in the mid 2010s likely reflects the projected Asian aerosol emissions' peak in the 2010s and BMB decline in South America, Southeast Asia (Takemura et al., 2012), and NH mid-latitude (see Fig. 4c in Chemke and Coumou, 2024) under RCP8.5. The difference between RCP8.5 and CMIP6 may help explain why Mode 2 shows smaller Asian AOD changes relative to the mid-latitudes, in contrast to the "shift" mode based on industrial aerosols from 1930-2010 identified by Wang and Wen (2020) using CMIP6, which showed comparable low- and mid-latitude contributions. These imply that regional emission variations, particularly in Asia, are crucial in shaping the dominant modes of global aerosol variability, and can shift the balance between atmospheric radiative and ocean-mediated pathways of aerosols, altering both the strength and spatial pattern of associated global climate responses. This further underscores the need to integrate evolving regional trajectories into future emission scenarios.

Having established the leading AOD modes, we next addressed two key questions: through which pathways do aerosols influence climate, and how do these pathways differ across regions and aerosol modes? By separating atmospheric radiative and ocean-mediated pathways, we showed that the ocean-mediated pathway tends to dominate the global large-scale circulation and precipitation responses to both AOD Modes, with offsetting contributions from the atmospheric radiative pathway. However, the interplay between the two pathways is complex and regionally dependent, making it difficult to generalize. NH land surface air temperature is an exception, where the two pathways have distinct roles in each mode. In Mode 1 (low-latitude aerosols), radiative forcing and SST-driven influences are comparable, whereas in Mode 2 (mid-latitude aerosols), radiative forcing dominates. This suggests that low-latitude aerosols can perturb local land surface air temperature through both pathways, making them efficient in driving regional changes. In contrast, mid-latitude aerosols primarily drive in-situ surface air temperature changes through the atmospheric radiative pathway. Although mid-latitude aerosols exert weaker local impacts, they have high efficacy in driving remote surface air temperature responses, including contributing to global mean surface air temperature (Shindell and Faluvegi, 2009; Persad and Caldeira, 2018).

The tropical Indo-Pacific and SH tropospheric circulation responses to AOD Mode 1 exemplify how low-latitude aerosols exert both local and remote influences on circulation through two pathways. The tropical Indo-Pacific sector displays a distinctive meridional dipole response in precipitation and tropospheric overturning circulation. The latitudinal structure of this response represents a hybrid between the broad cross-equatorial scale resulting from the ocean-mediated pathway, associated with remote and local aerosols (Bollasina et al., 2014; Undorf et al., 2018b), and the narrower NH dipolar pattern driven by the atmospheric radiative pathway, which likely reflects the influence of aerosols from adjacent sources (Fig. 5 in Persad, 2023). In the SH, both the radiatively forced and SST-driven responses produce poleward-propagating Rossby wave trains emanating from the tropics into the extratropics, but with opposite sign. Their largely canceling responses appear to be initiated by tropical diabatic heating anomalies from convection changes over the Sahel and tropical Indian Ocean in response to remote industrial aerosols, along with adiabatic heating anomalies associated with central Africa BMB aerosols in the atmospheric radiative case. These results suggest a potential aerosol-driven tropical–extratropical teleconnection in the SH, though confirmation with linear models or targeted experiments is needed.

Under the transient framework, we showed that the interplay of atmospheric radiative and ocean-mediated effects is neither uniform nor stationary. Radiative effects can exert not only short-lived adjustments but also persistent, decadal-scale influences. This blurs the conventional distinction between “fast” and “slow” responses to radiative forcing, as long-term evolving radiative forcing itself may encompass a slow component. With aerosol emissions expected to decline, and clean air legislation already enacted in some countries, it is critical to account for both atmospheric radiative and ocean-mediated components of aerosol effects when predicting regional hydroclimate and risks such as heat extremes, given the mobility and geography-dependent nature of their nuanced interplay.

Much remains to be understood about the mechanisms underlying the atmospheric radiative and ocean-mediated pathways of response to the two AOD Modes documented here, including the relative contributions of local *vs.* remote aerosol emissions and their mode dependence, warranting further analysis of our experiments. Our study has utilized one climate model (CESM1) and one (CMIP5) representation of historical time-evolving industrial and biomass burning aerosols, both of which have known strengths and shortcomings (e.g., Holland et al. 2024). Repeating our approach with other models and updated aerosol emissions inventories

File generated with AMS Word template 2.0

would be a useful next step for addressing structural and forcing uncertainty. Models with improved representation of aerosol microphysical processes and aerosol-cloud interactions, enhanced vertical and horizontal resolution, and interactive wildfire capabilities, may be especially valuable in this regard. Applying our protocol to regional aerosol forcing experiments such as those conducted as part of the Regional Aerosol Model Intercomparison Project (Wilcox et al. 2023) may yield additional mechanistic insights, although non-linear interactions between forcings in different regions may complicate the picture (Diao et al. 2025). Additionally, this work focuses on boreal summertime (JJA) signals, particularly those associated with NH monsoon circulations and mid-latitude large-scale precipitations. Although the long-term variation of JJA AOD patterns likely does not differ from that of the annual mean and other seasons, addressing the seasonality of both the forcing and the response (for example, boreal winter as in Diao et al., 2025) would be a worthwhile next step.

Looking forward, anthropogenic aerosol emissions are expected to undergo substantial changes. With continued air quality regulation in Asia and growing industrial activity in tropical regions, the center of aerosol emissions may shift to South Asia, South America, and Africa, though the timing of this transition remains uncertain (Scholten et al., 2024). This shift is especially concerning given the high hydrological sensitivity of the tropics and its ability to influence climate worldwide via teleconnections (Smith et al., 2016; Dittus, et al., 2021; Liu et al., 2024). Given the critical role of anthropogenic aerosols in shaping historical changes in regional precipitation over densely populated areas (White et al. 2025), there is an essential need to incorporate information on anticipated near-term and long-term changes in both industrial and biomass burning aerosol emissions into climate projections and risk assessments (Persad et al., 2023). Importantly, understanding the physical pathways by which aerosols impact global climate would not only improve our interpretation of historical climate trends, but also enhance the reliability of future projections in a world increasingly shaped by GHGs and shifting aerosol regimes.

Acknowledgements

This work was supported by funding from the National Science Foundation (NSF) under award #2235177. This material and the CESM project are based on work supported by the National Center for Atmospheric Research (NCAR), which is a major facility sponsored by the

File generated with AMS Word template 2.0

NSF under Cooperative Agreement 1852977. Computations and data storage resources were provided by the Computational and Information Systems Laboratory (CISL) at NCAR.

Data Availability Statement.

The CESM1 CAM5 AMIP single-forcing experiment data will be available through a NCAR GLOBUS guest collection. The CESM1 Large Ensemble simulations used in this study are available from http://www.cesm.ucar.edu/experiments/cesm1.1/LE/#single-forcing and http://www.cesm.ucar.edu/projects/community-projects/LENS.

REFERENCES

Allen, R. J., A. T. Evan, and B. B. B. Booth, 2015: Interhemispheric Aerosol Radiative Forcing and Tropical Precipitation Shifts during the Late Twentieth Century. J. Climate, 28, 8219–8246, https://doi.org/10.1175/JCLI-D-15-0148.1.

Allen, R.J., Vega, C., Yao, E., and Liu, W., 2024: Impact of industrial versus biomass burning aerosols on the Atlantic Meridional Overturning Circulation. npj Climate and Atmospheric Science, 7(1), p.58, https://doi.org/10.1038/s41612-024-00602-8.

Ashok, K., Guan, Z. and Yamagata, T., 2003: Influence of the Indian Ocean Dipole on the Australian winter rainfall, Geophys. Res. Lett., 30, 1821, doi:10.1029/2003GL017926, 15.

Bala, G., Caldeira, K., and Nemani, R., 2010: Fast versus slow response in climate change: implications for the global hydrological cycle. *Climate dynamics*, *35*, pp.423-434, https://doi.org/10.1007/s00382-009-0583-y.

Berbery, E. H., J. Nogués-Paegle, and J. D. Horel, 1992: Wavelike Southern Hemisphere Extratropical Teleconnections. *J. Atmos. Sci.*, **49**, 155–177, https://doi.org/10.1175/1520-0469(1992)049<0155:WSHET>2.0.CO;2.

Bollasina, M.A., Ming, Y. and Ramaswamy, V., 2011: Anthropogenic aerosols and the weakening of the South Asian summer monsoon. Science, 334(6055), pp.502-505, DOI:10.1126/science.1204994

Bollasina, M.A., Ming, Y., Ramaswamy, V., Schwarzkopf, M.D. and Naik, V., 2014: Contribution of local and remote anthropogenic aerosols to the twentieth century weakening of the South Asian Monsoon. Geophys. Res. Lett., 41, 680–687, doi:10.1002/2013GL058183.

Booth, B.B., and Coauthors, 2012: Aerosols implicated as a prime driver of twentieth-century North Atlantic climate variability. *Nature*, *484*(7393), pp.228-232, https://doi.org/10.1038/nature10946.

Cai, W., D. Bi, J. Church, T. Cowan, M. Dix, and L. Rotstayn, 2006*:* Pan-oceanic response to increasing anthropogenic aerosols: Impacts on the Southern Hemisphere oceanic circulation. *Geophys. Res. Lett.*, ***33***, L21707, doi:10.1029/2006GL027513.

Cai, W., P. van Rensch, T. Cowan, and H. H. Hendon, 2011: Teleconnection Pathways of ENSO and the IOD and the Mechanisms for Impacts on Australian Rainfall. J. Climate, 24, 3910–3923, https://doi.org/10.1175/2011JCLI4129.1.

Chemke, R. and Coumou, D., 2024: Human influence on the recent weakening of storm tracks in boreal summer. *npj Climate and Atmospheric Science*, *7*(1), p.86, https://doi.org/10.1038/s41612-024-00640-2.

Cunningham, C.X., Williamson, G.J., and Bowman, D.M., 2024: Increasing frequency and intensity of the most extreme wildfires on Earth. Nature ecology & evolution, 8(8), pp.1420-1425, https://doi.org/10.1038/s41559-024-02452-2.

Dagan, G., Stier, P., and Watson-Parris, D., 2020: Aerosol forcing masks and delays the formation of the North Atlantic warming hole by three decades. *Geophysical Research Letters*, 47(22), p.e2020GL090778, https://doi.org/10.1029/2020GL090778.

Delworth, T. L., and K. W. Dixon, 2006*:* Have anthropogenic aerosols delayed a greenhouse gas-induced weakening of the North Atlantic thermohaline circulation? *Geophys. Res. Lett.,* **33,** L02606, doi:10.1029/2005GL024980.

DeRepentigny, P., Jahn, A., Holland, M.M., Kay, J.E., Fasullo, J., Lamarque, J.F., Tilmes, S., Hannay, C., Mills, M.J., Bailey, D.A., and Barrett, A.P., 2022: Enhanced simulated early 21st century Arctic sea ice loss due to CMIP6 biomass burning emissions. *Science Advances*, *8*(30), p.eabo2405, DOI:10.1126/sciadv.abo2405.

Deser, C., and Coauthors, 2020: Isolating the Evolving Contributions of Anthropogenic Aerosols and Greenhouse Gases: A New CESM1 Large Ensemble Community Resource. *J. Climate*, **33**, 7835–7858, https://doi.org/10.1175/JCLI-D-20-0123.1.

File generated with AMS Word template 2.0

Diao, C., Xu, Y., Hu, A., and Wang, Z., 2025: Contrasting the roles of regional anthropogenic aerosols from the western and eastern hemispheres in driving the 1980-2020 Pacific multi-decadal variations. *Atmospheric Chemistry and Physics*, *25*(4), pp.2167-2180, https://doi.org/10.5194/acp-25-2167-2025.

Ding, Q., and E. J. Steig, 2013: Temperature Change on the Antarctic Peninsula Linked to the Tropical Pacific. J. Climate, 26, 7570–7585, https://doi.org/10.1175/JCLI-D-12-00729.1.

Dittus, A.J., Hawkins, E., Robson, J.I., Smith, D.M., and Wilcox, L.J., 2021: Drivers of recent North Pacific decadal variability: The role of aerosol forcing. *Earth's Future*, *9*(12), p.e2021EF002249, https://doi.org/10.1029/2021EF002249.

Dong, B., Sutton, R.T., Shaffrey, L. and Harvey, B., 2022: Recent decadal weakening of the summer Eurasian westerly jet attributable to anthropogenic aerosol emissions. Nature Communications, 13(1), p.1148, https://doi.org/10.1038/s41467-022-28816-5.

Dong, B., Wilcox, L.J., Highwood, E.J. *et al.,* 2019: Impacts of recent decadal changes in Asian aerosols on the East Asian summer monsoon: roles of aerosol–radiation and aerosol–cloud interactions. *Clim Dyn* **53**, 3235–3256. https://doi.org/10.1007/s00382-019-04698-0.

Dong, Y., Kay, J. E., Deser, C., Capotondi, A., and Sanchez, S. C., 2024: Distilling the evolving contributions of anthropogenic aerosols and greenhouse gases to large-scale low-frequency surface ocean changes over the past century. *Geophysical Research Letters*, 51, e2024GL112020. https://doi.org/10.1029/2024GL112020.

England, M.R., Eisenman, I., Lutsko, N.J., and Wagner, T.J., 2021: The recent emergence of Arctic amplification. *Geophysical Research Letters*, 48(15), p.e2021GL094086, https://doi.org/10.1029/2021GL094086.

Fasullo, J.T., Lamarque, J.F., Hannay, C., Rosenbloom, N., Tilmes, S., DeRepentigny, P., Jahn, A., and Deser, C., 2022: Spurious late historical-era warming in CESM2 driven by prescribed biomass burning emissions. *Geophysical Research Letters*, 49(2), p.e2021GL097420, https://doi.org/10.1029/2021GL097420.

Gillett, Z. E., H. H. Hendon, J. M. Arblaster, H. Lin, and D. Fuchs, 2022: On the Dynamics of Indian Ocean Teleconnections into the Southern Hemisphere during Austral Winter. *J. Atmos. Sci.*, **79**, 2453–2469, https://doi.org/10.1175/JAS-D-21-0206.1.

File generated with AMS Word template 2.0

Gregory, J.M., Ingram, W.J., Palmer, M.A., Jones, G.S., Stott, P.A., Thorpe, R.B., Lowe, J.A., Johns, T.C. and Williams, K.D., 2004: A new method for diagnosing radiative forcing and climate sensitivity. *Geophysical research letters*, *31*(3), doi:10.1029/2003GL018747.

Heyblom, K.B., Singh, H.A., Rasch, P.J., and Hirasawa, H., 2023: Variability in biomass burning emissions weakens aerosol forcing due to nonlinear aerosol-cloud interactions. *Geophysical Research Letters*, *50*(11), p.e2022GL102685, https://doi.org/10.1029/2022GL102685.

He, J., and B. J. Soden, 2015: Anthropogenic Weakening of the Tropical Circulation: The Relative Roles of Direct CO2 Forcing and Sea Surface Temperature Change. *J. Climate*, **28**, 8728-8742, https://doi.org/10.1175/JCLI-D-15-0205.1.

Hill, S. A., Y. Ming, and I. M. Held, 2015: Mechanisms of Forced Tropical Meridional Energy Flux Change. *J. Climate*, **28**, 1725–1742, https://doi.org/10.1175/JCLI-D-14-00165.1.

Hirasawa, H., P. J. Kushner, M. Sigmond, J. Fyfe, and C. Deser, 2020: Anthropogenic Aerosols Dominate Forced Multidecadal Sahel Precipitation Change through Distinct Atmospheric and Oceanic Drivers. *J. Climate*, **33**, 10187-10204, https://doi.org/10.1175/JCLI-D-19-0829.1.

Holland, M.M., Hannay, C., Fasullo, J., Jahn, A., Kay, J.E., Mills, M., Simpson, I.R., Wieder, W., Lawrence, P., Kluzek, E., and Bailey, D., 2024: New model ensemble reveals how forcing uncertainty and model structure alter climate simulated across CMIP generations of the Community Earth System Model. *Geoscientific Model Development*, *17*(4), pp.1585-1602, https://doi.org/10.5194/gmd-17-1585-2024.

Hoskins, B. J., and T. Ambrizzi, 1993: Rossby Wave Propagation on a Realistic Longitudinally Varying Flow. *J. Atmos. Sci.*, **50**, 1661-1671, https://doi.org/10.1175/1520-0469(1993)050<1661:RWPOAR>2.0.CO;2.

Hua, W., Dai, A., Zhou, L., Qin, M. and Chen, H., 2019: An externally forced decadal rainfall seesaw pattern over the Sahel and southeast Amazon. *Geophysical Research Letters*, 46, 923–932, https://doi.org/10.1029/2018GL081406.

Hua, W., Lou, S., Huang, X., Xue, L., Ding, K., Wang, Z., and Ding, A., 2024: Diagnosing uncertainties in global biomass burning emission inventories and their impact on modeled air pollutants, Atmos. Chem. Phys., 24, 6787–6807, https://doi.org/10.5194/acp-24-6787-2024.

Hwang, Y.-T., D. M. W. Frierson, and S. M. Kang, 2013: Anthropogenic sulfate aerosol and the southward shift of tropical precipitation in the late 20th century. *Geophys. Res. Lett.*, 40, 2845–2850, doi:10.1002/grl.50502.

Hwang, Y.T., Xie, S.P., Chen, P.J., Tseng, H.Y., and Deser, C., 2024: Contribution of anthropogenic aerosols to persistent La Niña-like conditions in the early 21st century. *Proceedings of the National Academy of Sciences*, *121*(5), p.e2315124121, https://doi.org/10.1073/pnas.2315124121.

IPCC AR6: Szopa, S., Naik, V., Adhikary, B., Artaxo, P., Berntsen, T., Collins, W.D., Fuzzi, S., Gallardo, L., Kiendler-Scharr, A., Klimont, Z. and Liao, H., 2021: Short-Lived Climate Forcers (Chapter 6).

Kang, J.M., Shaw, T.A. and Sun, L., 2024: Anthropogenic aerosols have significantly weakened the regional summertime circulation in the Northern Hemisphere during the satellite era. *AGU Advances*, 5, 2024AV001318, https://doi.org/10.1029/2024AV001318.

Kang, S.M., Xie, S.P., Deser, C., and Xiang, B., 2021: Zonal mean and shift modes of historical climate response to evolving aerosol distribution. *Science Bulletin*, *66*(23), pp.2405-2411, https://doi.org/10.1016/j.scib.2021.07.013.

Kay, J. E., and Coauthors, 2015: The Community Earth System Model (CESM) Large Ensemble Project: A Community Resource for Studying Climate Change in the Presence of Internal Climate Variability. *Bull. Amer. Meteor. Soc.*, **96**, 1333–1349, https://doi.org/10.1175/BAMS-D-13-00255.1.

Lawrence, D.M., and Coauthors, 2011: Parameterization improvements and functional and structural advances in version 4 of the Community Land Model. *Journal of Advances in Modeling Earth Systems*, *3*(1), doi:10.1029/2011MS00045.

Lamarque, J.-F., Bond, T. C., Eyring, V., Granier, C., Heil, A., Klimont, Z., Lee, D., Liousse, C., Mieville, A., Owen, B., Schultz, M. G., Shindell, D., Smith, S. J., Stehfest, E., Van Aardenne, J., Cooper, O. R., Kainuma, M., Mahowald, N., McConnell, J. R., Naik, V., Riahi, K., and van Vuuren, D. P.: Historical (1850–2000) gridded anthropogenic and biomass burning emissions of reactive gases and aerosols: methodology and application, Atmos. Chem. Phys., 10, 7017–7039, https://doi.org/10.5194/acp-10-7017-2010.

File generated with AMS Word template 2.0

Li, S., Liu, W., Allen, R.J., Shi, J.R. and Li, L., 2023: Ocean heat uptake and interbasin redistribution driven by anthropogenic aerosols and greenhouse gases. *Nat. Geosci.*, *16*(8), pp.695-703, https://doi.org/10.1038/s41561-023-01219-x.

Li, X., Ting, M., You, Y., Lee, D.-E., Westervelt, D. M., & Ming, Y., 2020: South Asian summer monsoon response to aerosol-forced sea surface temperatures. Geophysical Research Letters, 47, e2019GL085329. https://doi.org/10.1029/2019GL085329.

Li, Y., J. Li, F. F. Jin, and S. Zhao, 2015: Interhemispheric Propagation of Stationary Rossby Waves in a Horizontally Nonuniform Background Flow. *J. Atmos. Sci.*, **72**, 3233–3256, https://doi.org/10.1175/JAS-D-14-0239.1.

Li, X., Cai, W., Meehl, G.A. et al., 2021: Tropical teleconnection impacts on Antarctic climate changes. Nat Rev Earth Environ 2, 680–698, https://doi.org/10.1038/s43017-021-00204-5.

Li, X., Ting, M. and Lee, D.E., 2018. Fast adjustments of the Asian summer monsoon to anthropogenic aerosols. Geophysical Research Letters, 45(2), pp.1001-1010. https://doi.org/10.1002/2017GL076667.

Liu, X., Easter, R.C., Ghan, S.J., Zaveri, R., Rasch, P., Shi, X., Lamarque, J.F., Gettelman, A., Morrison, H., Vitt, F., and Conley, A., 2012: Toward a minimal representation of aerosols in climate models: Description and evaluation in the Community Atmosphere Model CAM5. *Geoscientific Model Development*, *5*(3), pp.709-739, https://doi.org/10.5194/gmd-5-709-2012.

Liu, F., Li, X., Luo, Y., Cai, W., Lu, J., Zheng, X.T., Kang, S.M., Wang, H., and Zhou, L., 2024: Increased Asian aerosols drive a slowdown of Atlantic meridional overturning circulation. Nature Communications, 15(1), p.18, https://doi.org/10.1038/s41467-023-44597-x.

Liu, L., and Coauthors, 2018: A PDRMIP Multimodel Study on the Impacts of Regional Aerosol Forcings on Global and Regional Precipitation. *J. Climate*, **31**, 4429–4447, https://doi.org/10.1175/JCLI-D-17-0439.1.

Lund, M. T., Myhre, G., and Samset, B. H., 2019: Anthropogenic aerosol forcing under the Shared Socioeconomic Pathways, Atmos. Chem. Phys., 19, 13827–13839, https://doi.org/10.5194/acp-19-13827-2019.

File generated with AMS Word template 2.0

Menary, M.B., and Coauthors, 2020: Aerosol-forced AMOC changes in CMIP6 historical simulations. *Geophysical Research Letters*, *47*(14), p.e2020GL088166, https://doi.org/10.1029/2020GL088166.

Ming, Y., and V. Ramaswamy, 2011: A Model Investigation of Aerosol-Induced Changes in Tropical Circulation. *J. Climate*, **24**, 5125-5133, https://doi.org/10.1175/2011JCLI4108.1.

Morrison, H., and A. Gettelman, 2008: A New Two-Moment Bulk Stratiform Cloud Microphysics Scheme in the Community Atmosphere Model, Version 3 (CAM3). Part I: Description and Numerical Tests. *J. Climate*, **21**, 3642-3659, https://doi.org/10.1175/2008JCLI2105.1.

Mueller, B. L., N. P. Gillett, A. H. Monahan, and F. W. Zwiers, 2018: Attribution of Arctic Sea Ice Decline from 1953 to 2012 to Influences from Natural, Greenhouse Gas, and Anthropogenic Aerosol Forcing. *J. Climate*, **31**, 7771-7787, https://doi.org/10.1175/JCLI-D-17-0552.1.

Nabat, P., Somot, S., Boé, J., Corre, L., Katragkou, E., Li, S., Mallet, M., van Meijgaard, E., Pavlidis, V., Pietikäinen, J.P., and Sørland, S., 2025: Multi-model assessment of the role of anthropogenic aerosols in summertime climate change in Europe. *Geophysical Research Letters*, 52, e2024GL112474, https://doi.org/10.1029/2024GL112474.

Neale, R.B., Chen, C.C., Gettelman, A., Lauritzen, P.H., Park, S., Williamson, D.L., Conley, A.J., Garcia, R., Kinnison, D., Lamarque, J.F., and Marsh, D., 2010: Description of the NCAR community atmosphere model (CAM 5.0). *NCAR Tech. Note NCAR/tn-486+ STR*, *1*(1), pp.1-12.

Persad, G.G., and Caldeira, K., 2018: Divergent global-scale temperature effects from identical aerosols emitted in different regions. *Nature Communications*, *9*(1), p.3289, https://doi.org/10.1038/s41467-018-05838-6.

Persad, G. G., D. J. Paynter, Y. Ming, and V. Ramaswamy, 2017: Competing Atmospheric and Surface-Driven Impacts of Absorbing Aerosols on the East Asian Summertime Climate. J. Climate, 30, 8929–8949, https://doi.org/10.1175/JCLI-D-16-0860.1.

Persad, G.G., Cummins, C. and Baldwin, J.W., 2025: Anthropogenic aerosol changes disproportionately impact the evolution of global heatwave hazard and exposure. *Environmental Research Letters*, *20*(8), p.084023.

File generated with AMS Word template 2.0

Persad, G., Samset, B.H., Wilcox, L.J., Allen, R.J., Bollasina, M.A., Booth, B.B., Bonfils, C., Crocker, T., Joshi, M., Lund, M.T. and Marvel, K., 2023: Rapidly evolving aerosol emissions are a dangerous omission from near-term climate risk assessments. Environmental Research: Climate, 2(3), p.032001.

Roesch, C.M., Fons, E., Ballinger, A.P. *et al.,* 2025: Decreasing aerosols increase the European summer diurnal temperature range. *npj Clim Atmos Sci* **8**, 47. https://doi.org/10.1038/s41612-025-00922-3

Samset, B.H., Myhre, G., Forster, P.M., Hodnebrog, Ø., Andrews, T., Faluvegi, G., Flaeschner, D., Kasoar, M., Kharin, V., Kirkevåg, A., and Lamarque, J.F., 2016: Fast and slow precipitation responses to individual climate forcers: A PDRMIP multimodel study. *Geophysical research letters*, *43*(6), pp.2782-2791, doi:10.1002/2016GL068064.

Scholten, R.C., Veraverbeke, S., Chen, Y., and Randerson, J.T., 2024: Spatial variability in Arctic–boreal fire regimes influenced by environmental and human factors. *Nature Geoscience*, *17*(9), pp.866-873, https://doi.org/10.1038/s41561-024-01505-2.

Schumacher, D.L., Singh, J., Hauser, M., Fischer, E.M., Wild, M. and Seneviratne, S.I., 2024: Exacerbated summer European warming not captured by climate models neglecting long-term aerosol changes. *Communications Earth & Environment*, *5*(1), p.182, https://doi.org/10.1038/s43247-024-01332-8.

Shaw, T., Voigt, A., 2015: Tug of war on summertime circulation between radiative forcing and sea surface warming. Nature Geosci 8, 560–566, https://doi.org/10.1038/ngeo2449.

Shawki, D., Voulgarakis, A., Chakraborty, A., Kasoar, M., & Srinivasan, J., 2018: The South Asian monsoon response to remote aerosols: Global and regional mechanisms. Journal of Geophysical Research: Atmospheres, 123, 11,585–11,601, https://doi.org/10.1029/2018JD028623.

Shi, J., Kwon, Y., and Wijffels, S. E., 2022: Two Distinct Modes of Climate Responses to the Anthropogenic Aerosol Forcing Changes. *J. Climate*, **35**, 3445–3457, https://doi.org/10.1175/JCLI-D-21-0656.1.

Shindell, D., Faluvegi, G., 2009: Climate response to regional radiative forcing during the twentieth century. Nature Geosci 2, 294–300. https://doi.org/10.1038/ngeo473.

Smith, D.M., and Coauthors, 2016: Role of volcanic and anthropogenic aerosols in the recent global surface warming slowdown. *Nature Climate Change*, *6*(10), pp.936-940, https://doi.org/10.1038/nclimate3058.

Sutton, R., Dong, B. 2012: Atlantic Ocean influence on a shift in European climate in the 1990s. *Nature Geosci* **5**, 788–792. https://doi.org/10.1038/ngeo1595.

Takemura, T., 2012: Distributions and climate effects of atmospheric aerosols from the preindustrial era to 2100 along Representative Concentration Pathways (RCPs) simulated using the global aerosol model SPRINTARS, Atmos. Chem. Phys., 12, 11555–11572, https://doi.org/10.5194/acp-12-11555-2012.

Tian, Y., Hu, S., and Deser, C., 2023: Critical role of biomass burning aerosols in enhanced historical Indian Ocean warming. *Nature Communications*, *14*(1), p.3508, https://doi.org/10.1038/s41467-023-39204-y.

Undorf, S., M. A. Bollasina, and G. C. Hegerl, 2018a: Impacts of the 1900–74 Increase in Anthropogenic Aerosol Emissions from North America and Europe on Eurasian Summer Climate. *J. Climate*, **31**, 8381–8399, https://doi.org/10.1175/JCLI-D-17-0850.1.

Undorf, S., Polson, D., Bollasina, M. A., Ming, Y., Schurer, A., & Hegerl, G. C., 2018b: Detectable impact of local and remote anthropogenic aerosols on the 20th century changes of West African and South Asian monsoon precipitation. Journal of Geophysical Research: Atmospheres, 123, 4871–4889. https://doi.org/10.1029/2017JD027711.

Van Der Werf, G.R., Randerson, J.T., Giglio, L., Van Leeuwen, T.T., Chen, Y., Rogers, B.M., Mu, M., Van Marle, M.J., Morton, D.C., Collatz, G.J., and Yokelson, R.J., 2017: Global fire emissions estimates during 1997–2016. *Earth System Science Data*, *9*(2), pp.697-720, https://doi.org/10.5194/essd-9-697-2017.

Wang, H., and Wen, Y.J., 2022: Climate response to the spatial and temporal evolutions of anthropogenic aerosol forcing. *Climate Dynamics*, *59*(5), pp.1579-1595, https://doi.org/10.1007/s00382-021-06059-2.

Wang, H., S. Xie, Y. Kosaka, Q. Liu, and Y. Du, 2019: Dynamics of Asian Summer Monsoon Response to Anthropogenic Aerosol Forcing. J. Climate, 32, 843–858, https://doi.org/10.1175/JCLI-D-18-0386.1.

File generated with AMS Word template 2.0

Wang, H., Zheng, X., Cai, W., Han, Z., Xie, S., Kang, S.M., Geng, Y., Liu, F., Wang, C., Wu, Y. Xiang, B. & Zhou, L., 2024: Atmosphere teleconnections from abatement of China aerosol emissions exacerbate Northeast Pacific warm blob events, Proc. Natl. Acad. Sci. U.S.A. 121 (21) e2313797121, https://doi.org/10.1073/pnas.2313797121.

Wang, Z., Lin, L., Xu, Y., Che, H., Zhang, X., Zhang, H., Dong, W., Wang, C., Gui, K.. and Xie, B., 2021: Incorrect Asian aerosols affecting the attribution and projection of regional climate change in CMIP6 models. *npj Climate and Atmospheric Science*, *4*(1), p.2, https://doi.org/10.1038/s41612-020-00159-2.

Westervelt, D. M., You, Y., Li, X., Ting, M., Lee, D. E., & Ming, Y., 2020: Relative importance of greenhouse gases, sulfate, organic carbon, and black carbon aerosol for South Asian monsoon rainfall changes. Geophysical Research Letters, 47, e2020GL088363, https://doi.org/10.1029/2020GL088363.

White, K., G. Persad, Samset, B.H. and coauthors, 2025: Anthropogenic Aerosols Dominate the Forced Contribution to Historical Precipitation Trends in Populated Regions, *Proceedings of the National Academy of Sciences* (under review).

Wilcox, L.J., Allen, R.J., Samset, B.H., Bollasina, M.A., Griffiths, P.T., Keeble, J., Lund, M.T., Makkonen, R., Merikanto, J., O'Donnell, D., and Paynter, D.J., 2023: The regional aerosol model intercomparison project (RAMIP). *Geoscientific Model Development*, *16*(15), pp.4451-4479, https://doi.org/10.5194/gmd-16-4451-2023.

Xiang, B., Xie, S.P., Kang, S.M., and Kramer, R.J., 2023: An emerging Asian aerosol dipole pattern reshapes the Asian summer monsoon and exacerbates northern hemisphere warming. *npj Climate and Atmospheric Science*, *6*(1), p.77, https://doi.org/10.1038/s41612-023-00400-8.

Xie, S.P., Lu, B. and Xiang, B., 2013: Similar spatial patterns of climate responses to aerosol and greenhouse gas changes. *Nature Geosci*, *6*(10), pp.828-832, https://doi.org/10.1038/ngeo1931.

Zhang, Y., Shindell, D., Seltzer, K., Shen, L., Lamarque, J.-F., Zhang, Q., Zheng, B., Xing, J., Jiang, Z., and Zhang, L., 2021: Impacts of emission changes in China from 2010 to 2017 on domestic and intercontinental air quality and health effect, Atmos. Chem. Phys., 21, 16051–16065, https://doi.org/10.5194/acp-21-16051-2021.

File generated with AMS Word template 2.0